DOI: 10.1002/chem.200500036

# Low-Spin State Structure of $[Fe(chloroethyltetrazole)_6](BF_4)_2$ Obtained from Synchrotron Powder Diffraction Data

**Eva Dova,*[a] René Peschar,[a] Masaki Takata,[b] Eiji Nishibori,[c] Henk Schenk,[a] Arno F. Stassen,[d, e] and Jaap G. Haasnoot[d]**

**Abstract:** The complex $[Fe(teec)_6](BF_4)_2$ (teec = chloroethyltetrazole) shows a two-step complete spin-crossover transition in the temperature range 300–90 K. Time-resolved synchrotron powder diffraction experiments have been carried out in this temperature range, and crystal structure models have been obtained from the powder patterns by using the parallel tempering technique. Of these models, the low-spin state structure at 90 K has been refined completely with Rietveld refinement. Its structural characteristics are discussed in relation to the high-spin state model and other spin-crossover compounds. The complex shows a remarkable anisotropic unit-cell parameter contraction that is dependent on the applied cooling rate. In addition, the possible important implications for the interpretation of spin-crossover behavior in terms of structural changes are discussed.

**Keywords:** iron complexes · spin crossover · structure solution · X-ray diffraction

## Introduction

Spin crossover (SCO) is the phenomenon in which an external perturbation (e.g., temperature, light, or pressure) can change the spin state of an atom, thereby changing the total magnetic moment of the compound;[1–5] this may find potential application in areas such as temperature sensors, active elements in various types of molecular-based displays, and in information storage and retrieval.[1,6–10] A wide range of SCOs have been observed experimentally, for example, gradual complete, two-step transitions, transitions with a residual high-spin species at low temperature, and hysteresis loops.[11–13] Thermal SCO in coordination compounds of 3d transition metals has been well known for many years and, in particular, the compounds $[Fe(alkyltetrazole)_6]X_2$ ($X = BF_4^-$, $ClO_4^-$, $CF_3SO_3^-$) have been investigated in detail since their discovery in the early eighties,[14–15] because of their wide variety of SCO behavior.

Recently, a novel series of $Fe^{II}$ SCO complexes has been introduced with (halogen-ethyl)tetrazoles as ligands.[11,16] The series member $[Fe(chloroethyltetrazole)_6](BF_4)_2$ (**1**) shows a two-step spin transition between 300 and 90 K and it was hypothesized that two high-spin (HS) fractions of $Fe^{II}$ may exist with different crystallographic positioning and behavior during the spin transition.[11] A crystal structure determination of the HS structure from powder diffraction data revealed $Fe^{II}$ to be in a special position, but no evidence was found for different HS $Fe^{II}$ fractions.[17] The plateau in the transition curve has also been explained by the assumption that extra thermodynamic stabilization takes place when 50% of the $Fe^{II}$ ions are in the HS state and 50% in the low-spin (LS) state,[18] and in two recent articles this stabilization was attributed to the existence of regular structures of alternating HS and LS molecules.[19–20] To investigate this two-step phase transition in more detail from a structural point of view, synchrotron powder diffraction data have been collected at a series of temperatures along the

[a] Dr. E. Dova, Dr. R. Peschar, Prof. Dr. H. Schenk
University of Amsterdam, Faculty of Science
van't Hoff Institute for Molecular Sciences
Laboratory of Crystallography, Valckenierstraat 65
1018XE Amsterdam (The Netherlands)
Fax: (+31) 20-525-7041
E-mail: eva@science.uva.nl

[b] Prof. Dr. M. Takata
Japan Synchrotron Radiation Research Institute
Hyogo 679-5198 (Japan)

[c] Dr. E. Nishibori
Department of Applied Physics, Nagoya University
Nagoya 464-8603 (Japan)

[d] Dr. A. F. Stassen, Dr. J. G. Haasnoot
Leiden Institute of Chemistry, Leiden University
P.O. Box 9502, 2300 RA Leiden (The Netherlands)

[e] Dr. A. F. Stassen
Current address: Kavli Institute of Nanoscience
Delft University of Technology, Lorentzweg 1
2628 CJ Delft (The Netherlands)

  

spin-transition curve over two different time periods. By using the direct-space parallel tempering (simulated annealing) technique, crystal structure models have been obtained of which the model at 90 K has been refined completely. The crystal structure results and an analysis of the experimental data indicate that the changes in the structure that occur during the spin transition, as expressed by the unit-cell contraction, depend both on the average cooling rate and on the timescale of the data collection.

## Results

**Scan versus long-term measurement data**: The scan data show that peak positions and intensities change gradually as the temperature decreases (Figure 1), but neither changes in space group nor appearances of new peaks are observed, so a significant structural phase transition from 300→90 K is not likely to have occurred on this timescale.

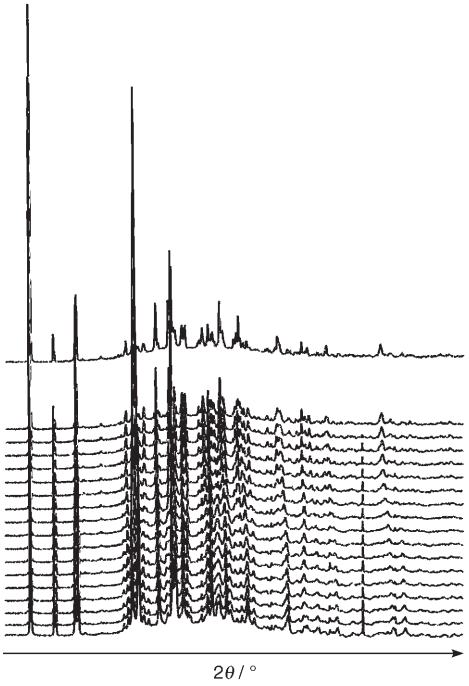


Figure 1. Diffraction patterns (3–35°=2$\theta$) of the scan measurements of $[Fe(teec)_6](BF_4)_2$: 300→90 K from top to bottom. Several changes in the peak positions and intensities can be observed.

As the temperature decreases, the unit-cell volume contraction follows the magnetic susceptibility versus temperature curve closely (Figure 2), in agreement with the findings of Meissner et al.[5] Interestingly, the volume contraction of the scan measurements shows the best correspondence. In this respect, it is worth noting that the average temperature drop ($\Delta T$) in the scan experiments (1.3 K min$^{-1}$, see Table 1) is comparable to the cooling rate used in the magnetic susceptibility measurements ($\approx$1 K min$^{-1}$). Some of the unit-

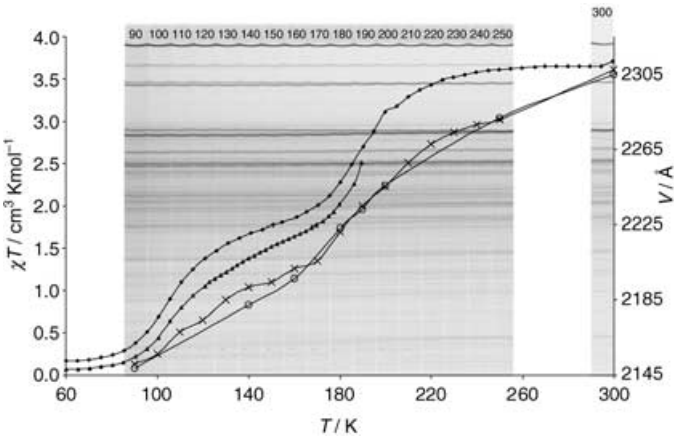


Figure 2. Unit-cell volume versus temperature for long-term (○) and scan (×) measurements of $[Fe(teec)_6](BF_4)_2$: the larger volume differences at the same temperature are observed after the plateau ($T\approx$150 K). Magnetic susceptibility ($\chi T$) of both batches A (◆) and B (▲) is plotted and the Imaging Plate picture of the scan measurements is shown too for comparison (see legend at top of the figure).

Table 1. Average temperature drop [K min$^{-1}$] in the scan and long-term experiments of $[Fe(teec)_6](BF_4)_2$.

| Scan measurements (5 min) | | Long-term measurements (60 min) | |
|---|---|---|---|
| step | $\Delta T$ | step | $\Delta T$ |
| 300→250 | 5.55 | 300→250, 250→200, 140→90 | 0.77 |
| rest | 1.3 | 200→190, 190→180 | 0.15 |
| | | 180→160, 160→140 | 0.31 |

cell parameters, in particular the angle $\beta$, the $a$ and $b$ axes, and the volume, are remarkably different in scan and long-term experiments, especially after the first step of the SCO ($T\approx$170 K; Table 2, Figure 3a and b). A possible explanation is the much lower cooling rate in the case of long-term measurements (at $T$=170 K, $\Delta T$=0.31 K min$^{-1}$, see Table 1) that may have resulted in thermal and structural stabilization.

In Figure 3c and d, for each temperature, the changes in unit-cell axis lengths ($\Delta L = L_T - L_{90}$) and volume ($\Delta V = V_T - V_{90}$) relative to the values at 90 K are shown for the scan and long-term measurements, respectively. Figure 3c shows to a good approximation a two-step behavior, but for Figure 3d this conclusion cannot be drawn, also because of the lack of experimental points along the second step of the spin transition. The unit-cell contraction is anisotropic and in the scan experiments (Figure 3e) the largest changes (relative to $T$=300 K) are observed at the $b$ axis (3.2 %). Surprisingly, the anisotropic contraction in the long-term experiments is different, with a relatively larger contraction of the $a$ axis (Figure 3f). No significant differences were observed in the relative changes of $c$ axis and volume.

**Structure determination from X-ray powder data**: A summary of the results after Pawley refinement and Rietveld refinement (RR) with both the Materials Studio suite and the

  

Table 2. Unit-cell dimensions of $[Fe(teec)_6](BF_4)_2$ on the basis of all scan measurements (SPring8), Guinier, and ESRF data at room temperature (Dova et al, 2001) after full-pattern decomposition with MRIA. The second line given at several temperatures denotes the unit cell of the long-term measurements (refined with MS).

| $T$ [K] | $a$ [Å] | $b$ [Å] | $c$ [Å] | $\beta$ [°] | $V$ [Å$^3$] |
|---|---|---|---|---|---|
| 90 | 11.9509(16) | 17.407(3) | 10.3463(13) | 92.064(12) | 2150.9(6) |
| | 11.8171(4) | 17.5389(4) | 10.3690(3) | 90.8123(15) | 2148.85(11) |
| 100 | 11.9704(18) | 17.415(4) | 10.3512(16) | 92.085(15) | 2156.5(7) |
| 110 | 12.011(2) | 17.419(4) | 10.368(2) | 92.08(2) | 2167.8(9) |
| 120 | 12.034(17) | 17.433(4) | 10.3715(16) | 92.170(16) | 2174.3(7) |
| 130 | 12.065(3) | 17.449(5) | 10.387(3) | 92.13(3) | 2185.1(10) |
| 140 | 12.0735(16) | 17.469(4) | 10.3977(17) | 92.025(17) | 2191.7(8) |
| | 11.9341(4) | 17.5775(5) | 10.4050(3) | 90.8032(16) | 2182.46(12) |
| 150 | 12.0608(15) | 17.498(4) | 10.4057(17) | 91.873(17) | 2194.8(8) |
| 160 | 12.0609(16) | 17.532(4) | 10.4170(17) | 91.661(17) | 2201.8(8) |
| | 11.9801(5) | 17.5995(7) | 10.4173(4) | 90.772(16) | 2196.2(4) |
| 170 | 12.0646(15) | 17.548(4) | 10.4223(16) | 91.350(14) | 2205.9(7) |
| 180 | 12.0683(15) | 17.621(3) | 10.4459(15) | 90.968(12) | 2221.0(6) |
| | 12.04465(13) | 17.6686(3) | 10.44625(19) | 90.5910(16) | 2222.97(7) |
| 190 | 12.0892(12) | 17.672(3) | 10.4603(11) | 90.739(8) | 2234.6(5) |
| | 12.06831(12) | 17.6939(3) | 10.45744(16) | 90.5112(13) | 2232.95(6) |
| 200 | 12.1136(12) | 17.6943(17) | 10.4746(11) | 90.581(8) | 2245.0(5) |
| | 12.10189(12) | 17.7231(2) | 10.46997(17) | 90.4326(14) | 2245.57(6) |
| 210 | 12.1365(14) | 17.7383(17) | 10.4869(12) | 90.397(9) | 2257.6(5) |
| 220 | 12.1490(12) | 17.7709(14) | 10.5036(9) | 90.179(13) | 2267.7(5) |
| 230 | 12.1558(12) | 17.8105(14) | 10.5035(8) | 90.07(3) | 2274.0(8) |
| 240 | 12.1646(15) | 17.8488(17) | 10.5042(10) | 90.09(3) | 2278.7(7) |
| 250 | 12.1529(13) | 17.8700(13) | 10.4952(9) | 90.195(9) | 2279.3(4) |
| | 12.15736(12) | 17.8463(2) | 10.51659(14) | 90.2864(12) | 2281.69(5) |
| 300 | 12.1630(13) | 17.9882(12) | 10.5472(8) | 90.496(6) | 2307.5(4) |
| | 12.1775(3) | 17.9411(3) | 10.5498(2) | 90.5700(16) | 2304.78(9) |
| Guinier | 12.2013(15) | 17.9994(13) | 10.5832(8) | 90.560(6) | 2324.1(4) |
| ESRF | 12.1977(7) | 17.9693(9) | 10.5668(5) | 90.548(4) | 2316.0(3) |

general structure analysis system (GSAS; see Experimental Section) is given in Table 3. To compensate for the expected volume contraction due to cooling and the Fe–N bond shortening due to the SCO, in the parallel tempering (PT) runs the Fe–N bonds were shortened. Structure determination with PT at all temperatures investigated ($T$ = 200–90 K), using the modified ESRF structure as the initial model, turned out to be relatively easy. In all PT runs using 18 DOF (degrees of freedom) the $R_{wp}$ dropped significantly within 15 frames (20000 steps) from ≈14 to ≈9.5%, and in general, in less than 25 frames (1000000 steps) the final solution was found. A superposition (Figure 4) of all final structural models found in the PT runs and the structure solution determined from the ESRF data shows the similarity of the Fe–tetrazole ring conformations and also the much larger conformational variation of the chloroethyl groups.

The initial RRs were carried out at the chosen temperatures with the program package Materials Studio (MS) treating every chloroethyltetrazole branch (Figure 5) as a rigid body (see Experimental Section). The refinement of the 90 K model was carried out completely by using GSAS, because of its more sophisticated restraints handling and because it allows the refinement of a second phase. As a result of ice formation outside the capillary, the hexagonal ($P6_3/mmc$) phase of ice[21] with $a = b = 4.523$, $c = 7.367$ Å was introduced into the RR as a second phase. After fitting the ice phase using the same profile function as for the main phase, all its parameters were kept constant and only those of **1** were refined. Atomic displacement parameters (adps) of Cl could be refined isotropically but attempts to refine those of the other non-hydrogen atoms led to unacceptable values and therefore they were kept fixed at 0.025 Å$^2$ (default value in GSAS). Spherical harmonics coefficients up to the 6th order were refined and the final texture index was $J = 2.027$, implying a significant preferred orientation. The final observed and calculated diffraction patterns show a good correspondence, even in the higher angular region, as judged from the difference pattern (Figure 6).

A superposition of the final model refinement with GSAS and the final rigid-body-refined model with MS (Figure 7) and the difference in R values (Table 3) show that the model, although being restrained, has changed considerably, indicating the importance of imposing soft constraints and the limitation of the rigid-body approach.

**Structure of $[Fe(chloroethyltetrazole)_6](BF_4)_2$**: The $Fe^{II}$ ion in the centrosymmetric $[Fe(teec)_6]^{2+}$ complex is at a special position and is almost perfectly octahedrally coordinated to the neighboring nitrogen atoms at distances of 2.201(16)-2.220(16) Å at room temperature (RT) and of 1.813(10)–1.962(10) Å at 90 K, which are typical Fe–N distances at HS and LS states, respectively. Also, the N-Fe-N angles show an almost ideal octahedral symmetry with a maximum deviation of 0.8° from 90° at RT and 2.4° at 90 K. At RT, the four in-plane N atoms form an almost perfect square (deviation smaller than 1° from 90°). At 90 K, the square is distorted with a maximum deviation of 4.5° from 90° (distances and angles given in the text containing estimated standard deviations (esds) have been calculated with the program PLATON;[22] those not containing esds have been calculated with DIAMOND[23,24] or PLUVA).[25]

The average bond length of the Fe moiety (excluding the Fe–N bonds) at RT (1.29 Å) and at 90 K (1.28 Å) is virtually the same, so overall hardly any shrinkage has occurred as a result of the drop in temperature. In contrast, the average Fe–N bond decrease is 13.9% (0.31 Å), suggesting that the shortening of the Fe–N bonds is related to the HS→LS transition, as commonly observed with SCO compounds.[26]

  

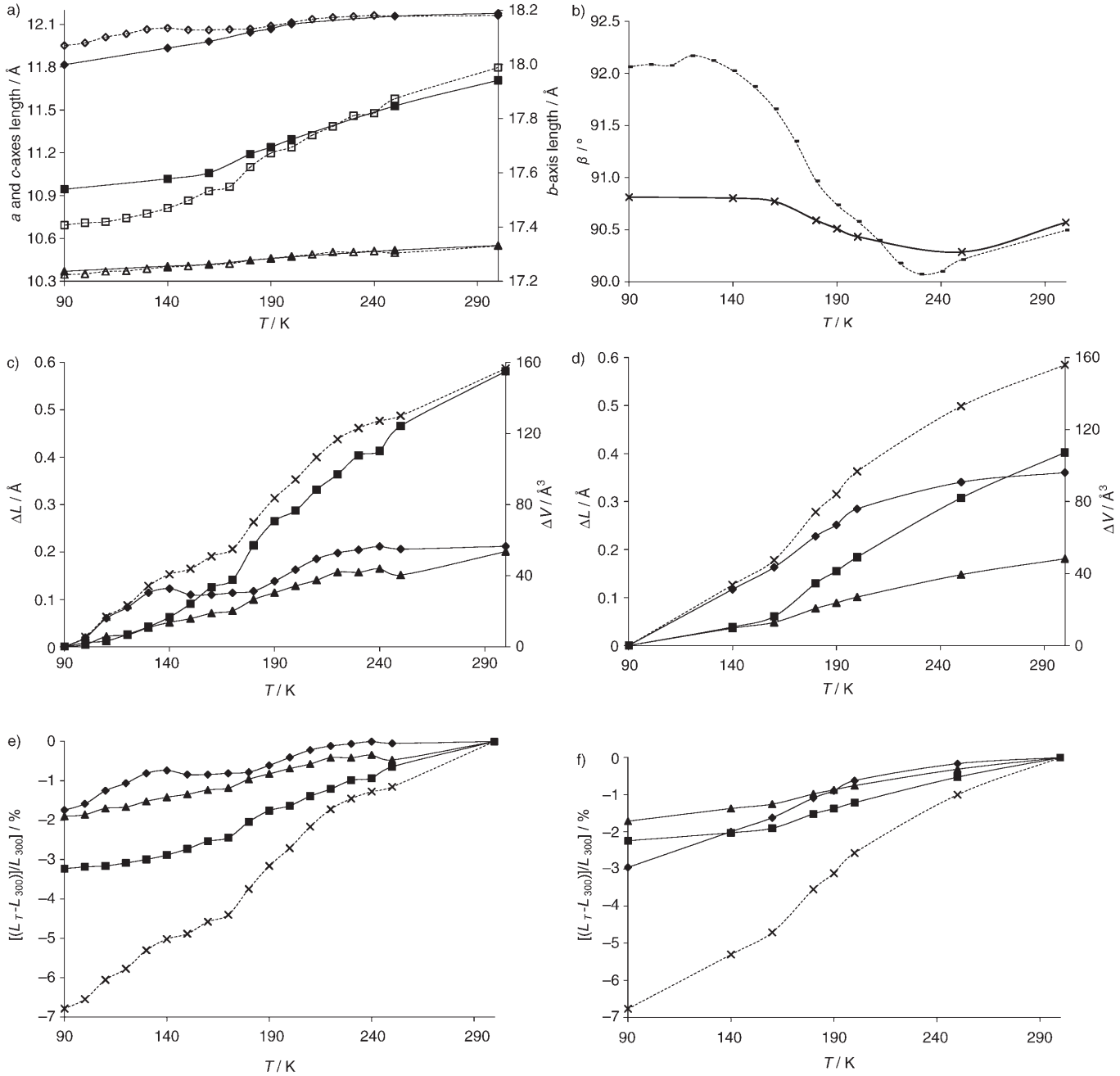


Figure 3. a) Unit-cell axes lengths (◆/◇ = long-term measurement (long)/scan measurement (scan), *a* axis; ▲/△ = long/scan, *c* axis; ■/□ = long/scan, *b* axis) and b) angle $\beta$ (× = long, – = scan) of the $[Fe(teec)_6](BF_4)_2$ unit cells as a function of temperature. Changes in unit-cell axes (◆ = *a*, ■ = *b*, ▲ = *c*) and volume (×) at each temperature relative to the values at c) 90 K (scan), d) 90 K (long), e) 300 K (scan), and f) 300 K (long).

From the superposition of the refined structures at RT and 90 K (Figure 8, left) it is concluded that, apart from the Fe–N contraction, the orientations of the tetrazole rings have hardly changed, as they are seen as being almost parallel at both temperatures. However, the ethyl molecules of the ligands have undergone much larger changes, especially the ethyl molecule of ligand c.

At both temperatures, the structure is packed in layers, parallel to the *b* and *c* axes and perpendicular to the *a* axis (Figure 9). Within the layers, the Fe and B atoms are centers of pseudotrigonal symmetry (Figure 10). The two structures differ significantly in the direction of the *b* and *c* axes, mainly because of the different position of the ethyl molecule of ligand c. The interlayer distance becomes shorter, from ≈2.9 Å at RT to 2 Å at 90 K. (It should be noted that the reported interlayer distances have been estimated visually as the layers being viewed along the *b* and *c* axes, therefore they are given for indicative and mostly comparative reasons.) Weak interlayer interactions seem to exist between close Cl and H atoms (Table 4). In Table 5, possible inter-

  

Table 3. Results of Pawley refinement (MS) and Rietveld refinement (MS, GSAS) as obtained for the SPring8 long-term measurements of $[Fe(teec)_6](BF_4)_2$.

| $T$ [K] | 200 | 180 | 160 | 140 | 90 |
|---|---|---|---|---|---|
| $R_p$[a,c] [%] | 3.65 | 3.72 | 3.93 | 3.81 | 2.36; 3.93 |
| | 1.20 | 1.21 | 1.11 | 1.15 | 1.07 |
| $R_{wp}$[b,c] [%] | 5.23 | 5.25 | 5.48 | 5.34 | 3.21; 5.45 |
| | 1.79 | 1.86 | 1.69 | 1.82 | 1.75 |
| $2\theta$ region[c] [°] | 3–55 | 3–52 | 3–52 | 3–51.5 | 2.5–47 |
| | 3–35 | 3–35 | 3–30 | 3–35 | 3–35 |
| resolution [Å] | 1.08 | 1.14 | 1.14 | 1.15 | 1.25 |
| | 1.66 | 1.66 | 1.93 | 1.66 | 1.66 |
| excluded regions [°] | | | 16.68–16.76 | 15.65–15.70 | 15.67–15.78 |
| | | | 27.85–27.93 | 25.64–25.74 | 16.65–16.80 |

[a] $R_p = \Sigma |y_{obsd} - y_{calcd}| / \Sigma y_{obsd}$. [b] $R_{wp} = \{\Sigma w(y_{obsd} - y_{calcd})^2 / \Sigma w y_{obsd}^2\}^{1/2}$. [c] The first line of $2\theta$ region, $R_p$, and $R_{wp}$ lists the settings and results of the Rietveld refinement (GSAS; MS results at 90 K), whereas the second line lists the settings and results of the FPD procedure.

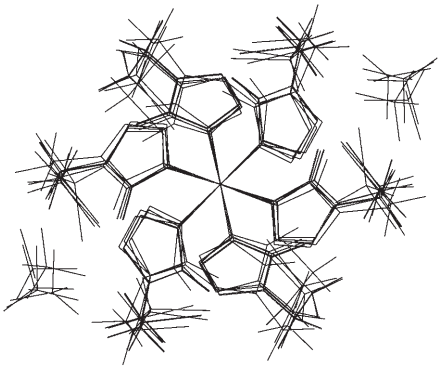

Figure 4. Superposition of structure solutions of $[Fe(teec)_6](BF_4)_2$ at all investigated temperatures after the parallel tempering procedure (SPring8 data) and the structure at RT from ESRF data.

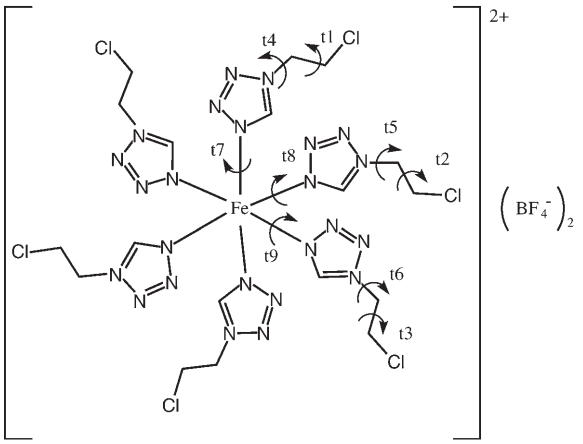


Figure 5. Torsion-angle (t1-t9) variations of chloroethyltetrazole moieties in $[Fe(teec)_6](BF_4)_2$.

molecular hydrogen bonds are listed. The N···H–C hydrogen bonds are directed almost parallel to the *b* axis and become weaker at 90 K. At 90 K, two Cl···H–C hydrogen bonds oriented almost parallel to the *c* axis have been formed, probably after the significant move of the chloroethyl of ligand c. Both of these Cl···H–C hydrogen bonds involve the b and c ligands of neighboring molecules along the *c* axis.

## Discussion

**Spin-crossover behavior**: The two-step magnetic susceptibility ($\chi T$) curves of two batches (A and B) of **1** and the presence of two different HS signals (HS1 and HS2) in the $^{57}Fe$ Mössbauer spectra of a third batch (C) have been explained by assuming the existence of two symmetry-inequivalent $Fe^{II}$ sites, each showing a different SCO behavior.[16] In other compounds, for example, in $[Fe(mtz)_6]X_2$ (mtz = methyltetrazole),[27] $[Fe(btr)_3](ClO_4)_2$ (btr = 4,4′-bis(1,2,4-triazole)),[28] and $[Fe(DPEA)(bim)](ClO_4)_2 \cdot 0.5\,H_2O$ (DPEA = 2-aminoethylbis(2-pyridylmethyl)amine, bim = 2,2-bisimidazole),[29] a similar type of argument was used based on single-crystal structure analyses. However, in **1** the fraction ($\gamma$HS) of $Fe^{II}$ ions in the HS1 and the HS2 states, as calculated from the $^{57}Fe$ Mössbauer experiment,[18] does not suggest two inequivalent sites of equal population, as this implies that one of the signals had to disappear first in the cooling mode.

As an alternative explanation of the two-step transition, it has been proposed that extra thermodynamic stabilization takes place when 50% of the $Fe^{II}$ ions are in the HS state and 50% in the LS state, as suggested by the plateau at $T \approx 155$ K.[18] In refs. [19,20] the spin crossover behavior of **1** was described quantitatively by two models, both based on the assumption that HS–LS structures are stabilized.

The first of these, the model of ordering, treats the stabilization as a result of nonspecific molecular interactions, that is, those that do not introduce any stoichiometric relationships and can be of any nature, for example, coulombic, hydrogen bonding, or delocalization of electrons. These interactions may be of different strength in homo- (HS–HS or LS–LS) and heteropairs (HS–LS). When ordering is taken into account, that is, the formation of regular structures with alternating LS and HS molecules, a plateau in the transition curve appears. In the approximation of binary interactions, only a qualitative correspondence between theoretical and experimental curves could be obtained. A quantitative description of the two-step spin crossover could be achieved only under the assumption of triple interactions, that is, interactions with the two nearest neighbors along a direction.

The second, the quasichemical model, considers the stabilization of HS–LS pairs to be the result of specific (stoichiometry-controlled) molecular interactions that occur through the rearrangements of ligands and associated energy levels. This purely chemical model (ideal approximation) provided a poor qualitative description of the two-step

  

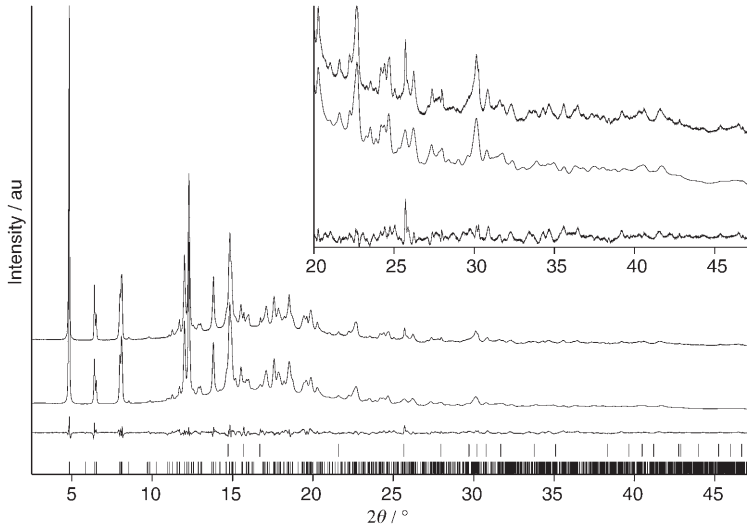


Figure 6. Experimental powder diffraction pattern at 90 K (top), the pattern calculated from the crystal structure after Rietveld refinement (middle), and the difference (exptl−calcd) pattern (bottom) of $[Fe(teec)_6](BF_4)_2$. The positions of ice peaks (upper row) and reflection positions (lower row) are marked by vertical lines. The inset shows an enlargement of the $2\theta = 20$–$45°$ region.

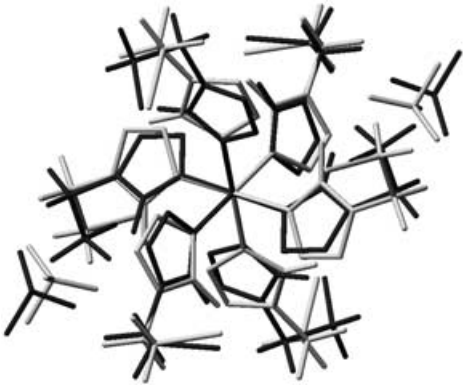

Figure 7. Superposition of the structure of $[Fe(teec)_6](BF_4)_2$ at 90 K after Rietveld Refinement with MS (light gray) and GSAS (black).

spin crossover, but when non-specific binary molecular interactions were also taken into account, an acceptable quantitative description was obtained.

In **1**, at all temperatures investigated ($T = 90$–$300$ K) the Fe atoms are at (symmetry-equivalent) special positions (space group $P2_1/c$, $Z = 2$) and there is no evidence from the performed diffraction experiments that at any moment the symmetry is broken or that the Fe atoms are behaving differently. Therefore, the two-step SCO behavior of **1** cannot be attributed to the existence of two types of differently behaving $Fe^{II}$ ions. The SPring-8 data of also provide no evidence that a structural phase transition is involved like in [Fe{5-$NO_2$-sal-N(1,4,7,10)}] (sal = salicylidene).[30] In fact, an explanation of the SCO solely on the basis of crystal structure similarity has limited applicability, as shown from $[Fe(mtz)_6](BF_4)_2$.[27] Like **1**, this compound is monoclinic, the cation complex is centrosymmetric, and the $Fe^{II}$ ions are at inversion centers. It is also layered with Fe and B exhibiting pseudotrigonal symmetry within the layers, following the general feature of the series $[Fe(Rtz)_6](BF_4)_2$ (R = alkyl),[31] and has Fe–B distances similar to those in **1**. In spite of these similarities, the magnetic behavior is different to $[Fe(mtz)_6](BF_4)_2$ in that it shows only a single-step SCO of 50% of the $Fe^{II}$ ions.

The SCO behavior of **1** resembles strongly that of $[Fe(2\text{-pic})_3]Cl_2 \cdot EtOH$[32] (**2**) which has been studied extensively

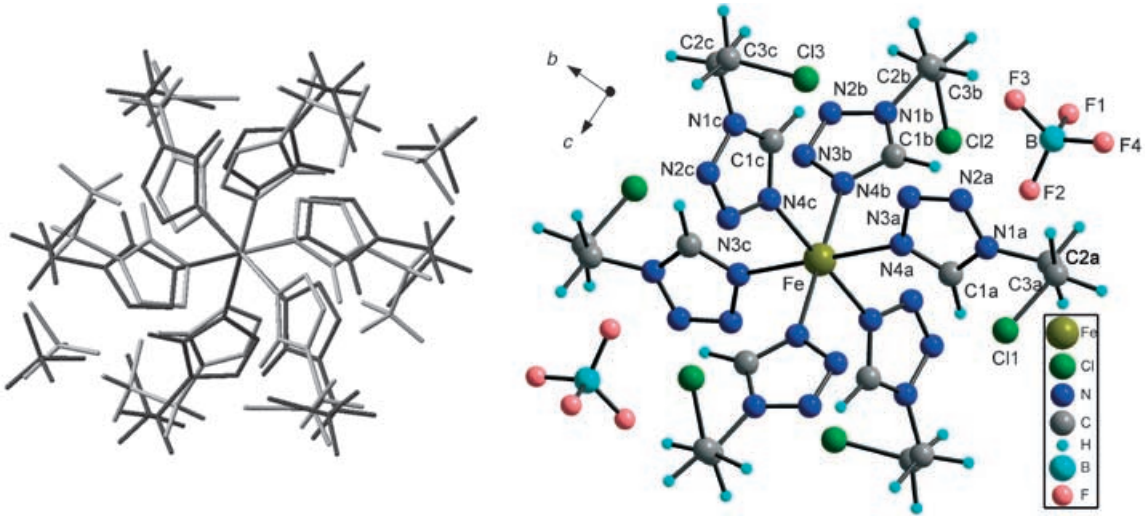


Figure 8. Left: The refined structures of $[Fe(teec)_6](BF_4)_2$ at RT (black) and 90 K (light gray) with an obvious shortening of the Fe–N bonds in the latter. Right: Molecular crystal structure of $[Fe(teec)_6](BF_4)_2$ showing the numbering scheme of the non-hydrogen atoms.

  

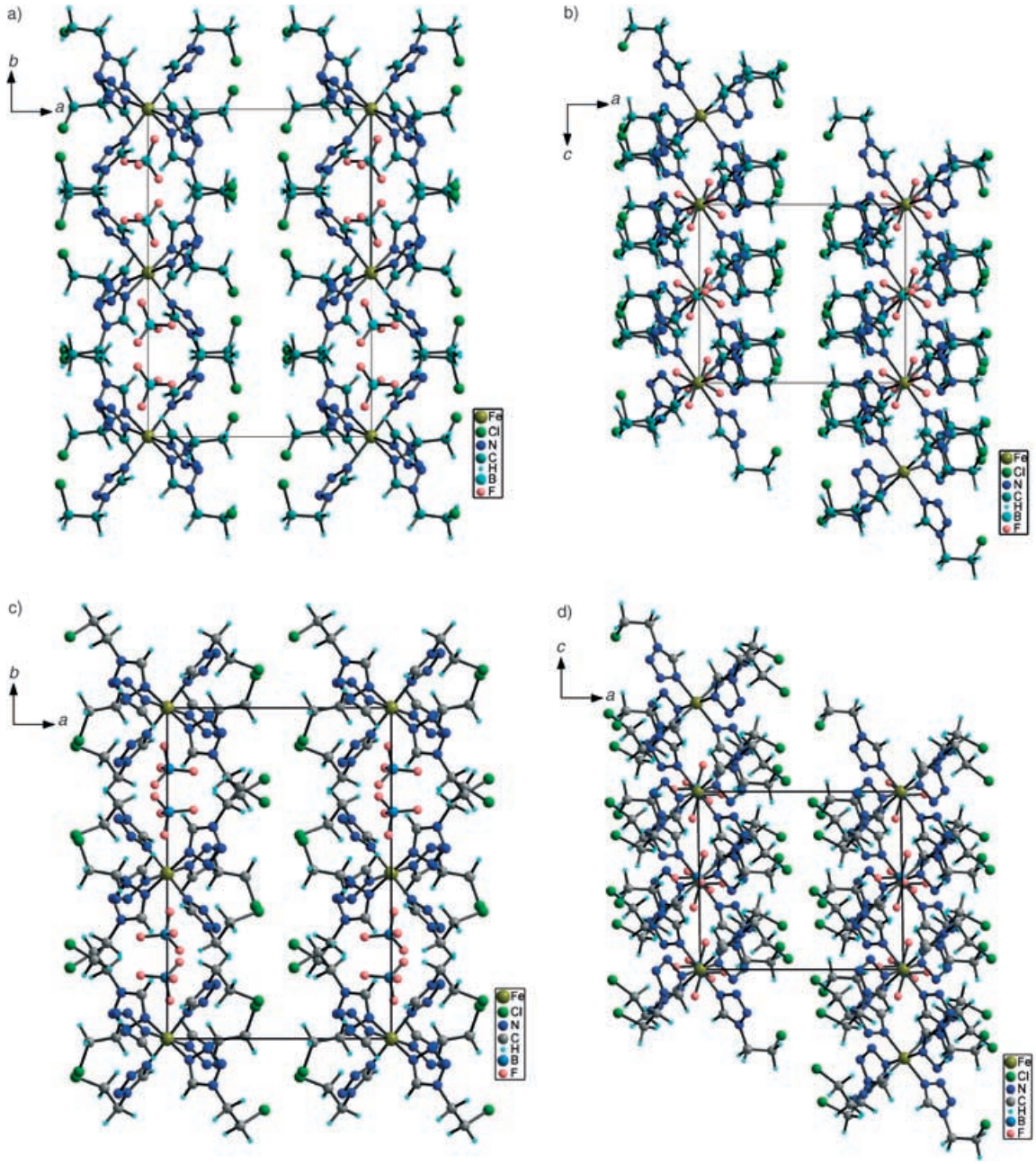


Figure 9. The structure of $[Fe(teec)_6](BF_4)_2$ at a),b) RT and c),d) 90 K showing the layers formed along the *b* and *c* axes (a),c), and b),d), respectively), perpendicular to the *a* axis.

since the first report about its spin transition by Renovitch and Baker.[33] By using single-crystal X-ray diffraction, crystal structures of **2** at various temperatures have been reported.[34–37] In both HS (298, 150 K) and LS (90 K) states the space group is $P2_1/c$ and no structural phase transition was observed.[35] A comparison of **1** with **2** shows $Fe^{II}$ to have a pseudooctahedral coordination (**2**) or an almost perfect octahedral coordination (**1**) through six N atoms, from three bidentate 2-picolylamine ligands (**2**) or six monodentate chloroethyl-tetrazole (**1**) ligands, respectively. When going from a HS to LS state, the Fe–N bonds contract on average by 0.18 Å (**2**) whereas in **1** the contraction is much larger (0.31 Å). The other bond lengths, however, do not change significantly in either case. Both **1** and **2** are packed in layers along the *b* and *c* axes that weakly interact along the *a* axis. In the layers of **2**, N–H···Cl and O–H···Cl hydrogen bonds form a two-dimensional hydrogen-bonding network parallel to the (001) plane. In the HS state, stronger N–H···Cl hydrogen bonds are present along the *c* axial direction, while in the LS state the ordering of the ethanol causes stronger O–H···Cl hydrogen bonds, so creating a stronger network along the *b* axis.[35] The hydrogen-bond networks in **1** and **2** are quite similar and although in **1** no definite hydrogen bonds have been assigned between $BF_4^-$ and the Fe

  

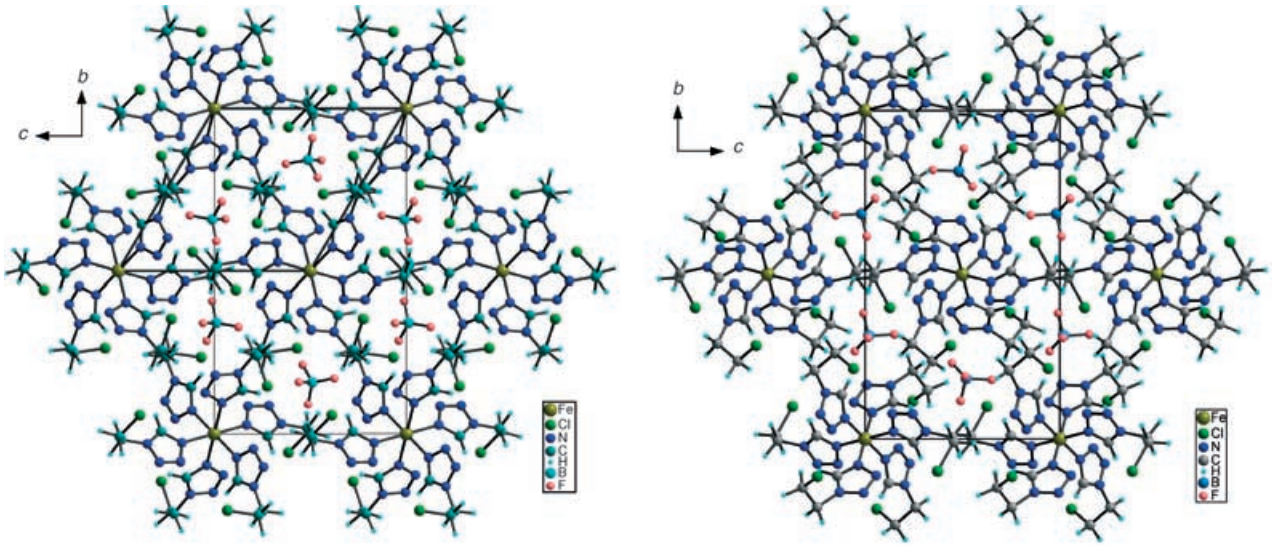


Figure 10. View of the $[Fe(teec)_6](BF_4)_2$ structure at RT (left) and 90 K (right) along the *a* axis; within these layers the Fe and B atoms exhibit pseudo-trigonal symmetry, shown with a thick line (left structure).

Table 4. Interlayer short contacts in $[Fe(teec)_6](BF_4)_2$ at RT and 90 K (the second line denotes the number of contacts in each case).

| *T* | Cl–Cl < 4.4 Å | Cl–H < 3.5 Å | H–H < 3.5 Å |
|---|---|---|---|
| RT | 3.90–4.26 | 2.87–3.48 | 2.82–3.43 |
| | 2 | 5 | 3 |
| 90 K | 4.05–4.32 | 2.99–3.26 | 2.96–3.46 |
| | 4 | 2 | 3 |

Table 5. Possible intermolecular hydrogen-bond lengths [Å] and angles [°] of the $[Fe(teec)_6](BF_4)_2$ structure at RT and 90 K.

| | RT | | | 90 K | | |
|---|---|---|---|---|---|---|
| | N···H | N···C | N-H-C | N···H | N···C | N-H-C |
| N2a···H2b2–C2b | 2.29(3) | 3.13(3) | 134(3) | 2.73 | 3.57 | 133 |
| N2b···H2a1–C2a | 2.44(3) | 3.18(3) | 121(2) | | | |
| N2b···H3a2–C3a | 2.61(4) | 3.33(3) | 122(3) | 2.70 | 3.25 | 110 |
| N2c···H2c1–C2c | 2.64 | 3.39 | 127 | 3.40 | 3.51 | 87 |
| | | | | Cl···H | Cl···C | Cl-H-C |
| C3b···H3b2–Cl3 | | | | 2.76(3) | 3.677(19) | 144(3) |
| C3c···H3c2–Cl2 | | | | 2.75(3) | 3.541(19) | 128(2) |

moiety, because of the possible disorder of $BF_4^-$, C–H···F and N–H···F hydrogen bonds possibly exist, especially at 90 K in view of the F–C and F–N distances (both ≈3 Å) and the F–H distances that are slightly larger than 2 Å. In spite of the structural similarities observed between **1** and **2**, the latter seems to have a different structural behavior at lower temperatures, as recently presented.[38] Reinvestigation of **2** by using X-ray single-crystal diffraction analyses revealed that it undergoes a first-order phase transition on cooling from a HS phase via an intermediate phase to a LS phase. Structure solution at sixteen temperatures between 12 and 298 K showed that the unit-cell constants and atomic coordinates change discontinuously from the HS to the LS phase. The intermediate phase, with a double unit-cell volume compared with the HS and LS phases, has two Fe moieties per asymmetric unit, one predominantly in the HS state and the other predominantly in the LS state. The sequence of the three phases has been characterized as "re-entrant" in the sense that the unit cell corresponding to the HS phase is similar to that of the LS phase but differs from the intermediate phase. Over the time span that the diffraction experiments of **1** were carried out, and with the used instrumentation, no additional reflections indicating a superstructure could be observed, but this does not exclude the fact that other experiments may demonstrate such a behavior.

**Anisotropy of unit-cell contraction**: An anisotropic unit-cell contraction was observed during the scan measurements, with the *b* axis contracting more than the *a* axis, indicating a larger mobility along the former within the structural layers parallel to the *bc* plane, rather than in between them, and resulting in an increase of the angle $\beta$. For the long-term measurements, the contraction turned out to be directed differently: the shrinkage along the *a* axis was larger while the *b* axis seemed to have relaxed compared with the scan experiments (Figure 3a). The decrease of the *c* axis was essentially the same in both the scan and long-term experiments. Remarkably, the main differences in the lattice parameters are observed practically after completion of the first SCO. These differences between the scan and long-term measurements suggest that structural changes in the complex, if any, occur first within the layers and parallel to the *b* axis, proba-

  

bly facilitated by the hydrogen bonds along the *b* axis, but later perpendicular to the layers. This behavior may be explained as follows: after the SCO takes place, the modified lattice vibrations (mainly due to the Fe–N bond-length shrinkage) are transmitted to the rest of the molecule. The first way for the vibrations to be transmitted is within the *bc* planes, as the intralayer intermolecular contacts and interactions (hydrogen bonds) are stronger than the interlayer contacts. After the intralayer relaxation, the contractions occur in directions where more space is available, that is, along the *a* axis. If this hypothesis is correct, the time span of the scan measurements could have been such that the first part of the lattice vibrations was traced, while the long-term measurements revealed the later structural changes. Overall, the structural changes connected with the lattice contractions probably were not very large as the unit cells of the scan measurements could still be described by using the same space group.

Anisotropic changes in lattice parameters as a function of temperature have been observed in other compounds that exhibit a two-step SCO. The unit-cell constants of **2** (single-crystal data) showed a linear decrease as the temperature was lowered in the HS region, but after the spin-transition temperature region, abrupt changes took place: 1.3% shrinkage of the *b* axis and 0.7% elongation of the *a* axis (at the time these results were reported, a one-step SCO vs *T* was still considered to take place).[34] From calculated thermal expansion coefficients, the authors concluded that the thermal vibration was the largest in the [100] direction, along which no hydrogen bonds were present. The latter is in agreement with the long-term measurements of **1**, as along the *a* axis no significant hydrogen bonds exist. In ref. [38] it is reported that the unit-cell constants and atomic coordinates change discontinuously with changing temperature between HS and LS phases, but no further details are given concerning anisotropy in those changes. In the case of $[Fe(DPEA)(bim)](ClO_4)_2 \cdot 0.5H_2O$ (also exhibiting a two-step SCO) the unit-cell contraction was anisotropic as well, with cell-parameter reductions of 2.15, 0.03, and 1.94% for the *a*, *b*, and *c* axes, respectively.[29]

Anisotropic changes in lattice parameters that depend on the cooling rate do not seem to have been reported previously. Until now, little attention has been paid to the dependence of the SCO behavior on the cooling/heating rate, except for the quenching leading to HS-state trapping. Amongst the few cases we could find, König et al.[39] concluded, on the basis of magnetic susceptibility measurements and Mössbauer spectroscopy analyses, that the cooling rate is of importance to SCO behavior. However, the dependence on the cooling rate referred to the SCO behavior and not to changes in the crystal structure, the latter being unavailable at the time the work was reported.

## Conclusion

From the results of the time- and temperature-dependent powder diffraction experiments and crystal structure determination of **1**, it cannot be straightforwardly concluded whether the origin of the two-step SCO is due to intermolecular interactions ("elasticity of the medium"), as suggested in the regular solution model.[40–42] The X-ray diffraction patterns also showed no evidence that domains consisting of molecules with identical spin[43] were formed, at least no domains that were large enough to be observed in the diffraction pattern and not on the timescale at which the diffraction experiments were carried out. The hypothesis of Romstedt et al.,[44] that anisotropic changes in the lattice lead to anisotropy of molecular interactions, is in agreement with our observations. Moreover, it was observed that the average cooling rate is important, at least for the lattice contraction and, possibly, also for the changes that occur at the molecular level although this fact does not necessarily justify the theory of the regular solution. From this it is concluded that to analyze spin-crossover behavior in terms of (crystal) structural changes, the timescale of the diffraction-data collection ideally should correspond to that of the magnetic data. The structural features of a long-term, thermally stabilized model may well differ from the structures occurring under nonequilibrium conditions, and this implies that the SCO behavior of complexes with similar long-term structures is not necessarily similar (as observed in the case of **1** and $[Fe(mtz)_6](BF_4)_2$).

## Experimental Section

**X-ray powder data collection**: Out of the three batches of **1** (A, B, and C, all white powders), prepared as described by Stassen et al.,[16] batch B time-resolved synchrotron powder diffraction data were collected at the beam line BL02B2 of the Japan Synchrotron Radiation Research Institute (Nishi-Harima, Hyogo, Japan; referred to as SPring8), by using a large Debye–Scherrer camera (radius 286.5 mm). Cooling in the range 90–300 K was achieved by using a $N_2$ gas flow, with a temperature accuracy of about $\pm 1$–2 K and quench capacities of 100 K $min^{-1}$ (300–110 K) and 30 K $min^{-1}$ (110–90 K).[45] An imaging plate detector (IP, selected pixel size 50 μm) was mounted on the $2\theta$ arm, allowing several powder patterns (max 18) to be recorded on a single IP using a long vertical slit attached in front of the IP. A 0.4 mm capillary was mounted in the sample holder of the camera and rotated with a speed of 6° $min^{-1}$. The wavelength used was $\lambda = 0.999995$ Å. After each experiment the IP was read out by a BAS-2000 machine and the two-dimensional digital frame was integrated over sets of 51 pixels (2.55 mm on the IP) using local SPring8 software into a normal powder diffraction pattern ($0.01 < 2\theta < 76.61$°, step 0.01°).

Short scan exposures (5 min) were used to select an appropriate sample (having nongranular and sharp lines) and subsequently, at a series of temperatures (300 K, and from 250 to 90 K in steps of 10 K), data collection was carried out for 5 min at each temperature. To avoid temperature overshoot, a temperature-stabilization period was applied before starting each data collection. The temperature-stabilization time from 300 to 250 K was 240 s and for all lower temperatures 160 s. In total, 18 diffraction patterns were collected within almost 137 min.

After inspection of the results at several temperatures (300, 250, 200, 190, 180, 160, 140, and 90 K) long-term (60 min at each temperature)

  

data collections were carried out in one run, using a temperature-stabilization time of 5 min after cooling to the next temperature. From the temperature difference and the sum of temperature-stabilization period and data-collection time, the average temperature drop ($K\,min^{-1}$) for each experiment was calculated (Table 1). After the long-term experiments (8 h 35 min) had been carried out, the color of the sample had become pale.

**Structure solution and refinement**: All powder diffraction patterns could be indexed on a monoclinic cell ($P2_1/c$) with $Z=2$, just like the room temperature ($T=293$ K, RT) pattern collected at the European Synchrotron Research Facility (ESRF).[17] Unit cells of the scan and long-term experiments (Table 2) were refined by applying the Pawley refinement as incorporated in the program package Materials Studio (MS) of Accelrys.[46] The $2\theta$ regions corresponding to ice peaks (ice formed outside the capillary at lower temperatures) were excluded except for ice peaks very close to reflection peaks. The background was fitted with the default settings (20th order polynomial). In all first runs of the structure solution procedure, the profile was fitted with a Pearson-VII function but later the Tomandl Pseudo-Voigt profile function was adopted because of a more satisfactory fitting, and this latter function was used in additional structure solution runs and in the Rietveld refinement (RR). In some cases, asymmetry correction was applied according to the Bérar–Baldinozzi function.[47]

The initial search model was taken from the ESRF-room temperature model of **1**.[17] With $Z=2$, **1** being centrosymmetric and the $Fe^{II}$ at a special position, eighteen structural parameters (degrees of freedom, DOF) had to be determined, consisting of the position and orientation of $BF_4^-$ (6 DOF) and the orientation (3 DOF) and torsion angles (9 DOF, Figure 5) of three chloroethyltetrazole moieties. In the first run of the parallel tempering (PT) optimization procedure of the program Powder Solve,[48–49] all 18 DOF were used simultaneously whereas in some later runs the number of DOF allowed to vary was decreased. The interval 3–25° $2\theta$ was used with default settings, unless stated otherwise (see Table 3).

In all runs, RR was carried out with the refinement program available in the MS package. The $[Fe(teec)_6]^{2+}$ moiety and $BF_4^-$ were refined initially as rigid bodies and the torsion angles (see Figure 5) were refined as well. Texture correction was applied using the March–Dollase method as implemented in the MS package. In the version of the MS package available at the time this work was carried out, no sophisticated restraints handling was available, except for a rigid-body option. Refinement attempts without this option were not successful and led to distorted models. Therefore, a full-restrained refinement, including bond-distance, bond-angle, and planar restraints, was carried out with the program GSAS[50] using the interface EXPGUI,[51] but only for the LS model (90 K), because of limitations in time and the surprising differences between scan and long-term diffraction data, as was discussed above. A special type of pseudo-Voigt function (profile function type 3 in GSAS) was used to model reflection asymmetry. Texture was corrected for using spherical-harmonic functions. Zero-point correction and cell-parameter refinement were applied as well.

CCDC-259971 contains the supplementary crystallographic data for this paper. These data can be obtained free of charge from the Cambridge Crystallographic Data Centre via www.ccdc.cam.ac.uk/data_request/cif.

## Acknowledgements

The authors thank Prof. Dr. M. Sakata and Dr. K. Kato for their help during the powder diffraction experiments at SPring8 (JASRI, Japan). E.D. acknowledges Accelrys Inc. for allowing the use of the Materials Studio software for evaluation purposes.

[1] P. Gütlich, A. Hauser, H. Spiering, *Angew. Chem.* **1994**, *106*, 2109–2141; *Angew. Chem. Int. Ed. Engl.* **1994**, *33*, 2024–2054.
[2] P. Gütlich, A. Hauser, *Coord. Chem. Rev.* **1990**, *97*, 1–22.
[3] S. Decurtins, P. Gütlich, H. Spiering, A. Hauser, C. P. Köhler, *Chem. Phys. Lett.* **1984**, *105*, 1–4.
[4] S. Decurtins, P. Gütlich, K. M. Hasselbach, A. Hauser, H. Spiering, *Inorg. Chem.* **1985**, *24*, 2174–2178.
[5] E. Meissner, H. Köppen, H. Spiering, P. Gütlich, *Chem. Phys. Lett.* **1983**, *95*, 163–166.
[6] O. Kahn, J. Kröber, C. Jay, *Adv. Mater.* **1992**, *4*, 718–728.
[7] C. Jay, F. Grolière, O. Kahn, J. Kröber, *Mol. Cryst. Liq. Cryst. Sci. Technol. Sect. A* **1993**, *234*, 255–262.
[8] J. Kröber, E. Codjovi, O. Kahn, F. Grolière, C. Jay, *J. Am. Chem. Soc.* **1993**, *115*, 9810–9811.
[9] O. Kahn, C. Jay Martinez, *Science* **1998**, *279*, 44–48.
[10] P. Gütlich, Y. Garcia, H. A. Godwin, *Chem. Soc. Rev.* **2000**, *29*, 419–427.
[11] A. F. Stassen, M. Grunert, E. Dova, H. Schenk, G. Wiesinger, W. Linert, J. G. Haasnoot, J. Reedijk, *Eur. J. Inorg. Chem.* **2003**, 2273–2282.
[12] P. Guionneau, J.-F. Letard, D. S. Yufit, D. Chasseau, G. Bravic, A. E. Goeta, J. A. K. Howard, O. Kahn, *J. Mater. Chem.* **1999**, *9*, 985–994.
[13] J.-A. Real, I. Castro, A. Bousseksou, M. Verdaguer, R. Burriel, J. Linares, F. Varret, *Inorg. Chem.* **1997**, *36*, 455–464.
[14] P. L. Franke, PhD Thesis, Leiden (The Netherlands), **1982**.
[15] P. L. Franke, J. G. Haasnoot, A. P. Zuur, *Inorg. Chim. Acta* **1982**, *59*, 5–9.
[16] A. F. Stassen, E. Dova, J. Ensling, H. Schenk, P. Gütlich, J. G. Haasnoot, J. Reedijk, *Inorg. Chim. Acta* **2002**, *335*, 61–68.
[17] E. Dova, A. F. Stassen, R. A. J. Driessen, E. Sonneveld, K. Goubitz, R. Peschar, J. G. Haasnoot, J. Reedijk, H. Schenk, *Acta Crystallogr. Sect. B* **2001**, *57*, 531–538.
[18] A. F. Stassen, PhD Thesis, Leiden (The Netherlands), **2002**.
[19] A. B. Koudriavtsev, A. F. Stassen, J. G. Haasnoot, M. Grunert, P. Weinberger, W. Linert, *Phys. Chem. Chem. Phys.* **2003**, *5*, 3666–3675.
[20] A. B. Koudriavtsev, A. F. Stassen, J. G. Haasnoot, M. Grunert, P. Weinberger, W. Linert, *Phys. Chem. Chem. Phys.* **2003**, *5*, 3676–3683.
[21] H. D. Megaw, *Nature* **1934**, *134*, 900–901.
[22] A. L. Spek, PLATON, Utrecht University, Utrecht (The Netherlands), **2001**.
[23] W. T. Pennington, *J. Appl. Crystallogr.* **1999**, *32*, 1028–1029.
[24] G. Cordier, *Nachr. Chem. Tech. Lab.* **1999**, *47*, 1437–1438.
[25] R. A. J. Driessen, B. O. Loopstra, D. P. de Bruijn, H. P. C. E. Kuipers, H. Schenk, *J. Comput.-Aided Mol. Des.* **1988**, *2*, 225–233.
[26] E. König, *Prog. Inorg. Chem.* **1987**, *35*, 527–623.
[27] L. Wiehl, *Acta Crystallogr. Sect. B* **1993**, *49*, 289–303.
[28] Y. Garcia, O. Kahn, L. Rabardel, B. Chansou, L. Salmon, J. P. Tuchagues, *Inorg. Chem.* **1999**, *38*, 4663–4670.
[29] G. S. Matouzenko, J.-F. Létard, S. Lecocq, A. Bousseksou, L. Capes, L. Salmon, M. Perrin, O. Kahn, A. Collet, *Eur. J. Inorg. Chem.* **2001**, 2935–2945.
[30] D. Boinnard, A. Bousseksou, A. Dworkin, J.-M. Savariault, F. Varret, J.-P. Touchagues, *Inorg. Chem.* **1994**, *33*, 271–281.
[31] R. Hinek, H. Spiering, D. Schollmeyer, P. Gütlich, A. Hauser, *Chem. Eur. J.* **1996**, *2*, 1427–1434.
[32] H. Köppen, E. W. Müller, C. P. Köhler, H. Spiering, E. Meissner, P. Gütlich, *Chem. Phys. Lett.* **1982**, *91*, 348–352.
[33] G. A. Renovitch, W. A. Baker, Jr., *J. Am. Chem. Soc.* **1967**, *89*, 6377–6378.
[34] M. Mikami, M. Konno, Y. Saito, *Chem. Phys. Lett.* **1979**, *63*, 566–569.
[35] M. Mikami, M. Konno, Y. Saito, *Acta Crystallogr. Sect. B* **1980**, *36*, 275–287.
[36] A. M. Greenaway, C. J. O'Connor, A. Schrock, E. Sinn, *Inorg. Chem.* **1979**, *18*, 2692–2695.
[37] B. A. Katz, C. E. Strouse, *J. Am. Chem. Soc.* **1979**, *101*, 6214–6221.
[38] D. Chernyshov, M. Hostettler, K. W. Törnroos, H.-B. Bürgi, *Angew. Chem.* **2003**, *115*, 3955–3960; *Angew. Chem. Int. Ed.* **2003**, *42*, 3825–3830.

  

[39] E. König, G. Ritter, J. Dengler, S. M. Nelson, *Inorg. Chem.* **1987**, *26*, 3582–3588.
[40] C. P. Slichter, H. G. Drickamer, *J. Chem. Phys.* **1972**, *56*, 2142–2160.
[41] S. Onishi, S. Sugano, *J. Phys. C* **1981**, *14*, 39–55.
[42] H. Spiering, E. Meissner, H. Köppen, E. W. Müller, P. Gütlich, *Chem. Phys.* **1982**, *68*, 65–71.
[43] M. Sorai, S. Seki, *J. Phys. Chem. Solids* **1974**, *35*, 555–570.
[44] H. Romstedt, H. Spiering, P. Gütlich, *J. Phys. Chem. Solids* **1998**, *59*, 1353–1362.
[45] E. Nishibori, M. Takata, K. Kato, M. Sakata, Y. Kubota, S. Aoyagi, Y. Kuroiwa, M. Yamakata, N. Ikeda, *Nucl. Instrum. Methods Phys. Res. Sect. A* **2001**, *467–468*, 1045–1048.
[46] *Materials Studio*, Accelrys Inc., 6985 Scranton Road, San Diego, CA 92121-3752, USA, **2001**.
[47] J.-F. Bérar, J. Baldinozzi, *J. Appl. Crystallogr.* **1993**, *26*, 128–129.
[48] G. E. Engel, S. Wilke, O. Köning, K. D. M. Harris, F. J. J. Leusen, *J. Appl. Crystallogr.* **1999**, *32*, 1169–1179.
[49] G. A. Stephenson, *J. Pharm. Sci.* **2000**, *89*, 958–966.
[50] A. C. Larson, R. B. Von Dreele, *General Structure Analysis System (GSAS)*, Los Alamos National Laboratory Report, LAUR 86-748, **1994**.
[51] B. H. Toby, *J. Appl. Crystallogr.* **2001**, *34*, 210–213.

Received: January 13, 2005
Revised: April 11, 2005
Published online: July 25, 2005

  